Electronic Supplementary Material (ESI) for Journal of Materials Chemistry A.

Supporting information

Large-area, high-quality organic-inorganic hybrid perovskite thin films via controlled vapor-solid reaction

Xiaomin Chen,[a,b] Huanqi Cao,[*,a,b] Hao Yu,[a,b] Hao Zhu,[a,b] Huanping Zhou,[*,c] Liying Yang,[a,b] & Shougen Yin[*,a,b]

[a] *Key Laboratory of Display Materials and Photoelectric Devices (Ministry of Education), School of Materials Science and Engineering, Tianjin University of Technology, Tianjin 300384, China*

[b] *Tianjin Key Laboratory for Photoelectric Materials and Devices, School of Materials Science and Engineering, Tianjin University of Technology, Tianjin 300384, China*

[c] *Department of Materials Science and Engineering, College of Engineering, Peking University, 100871, China*

Growth-rate uniformity of perovskite films in tubular LPCVD

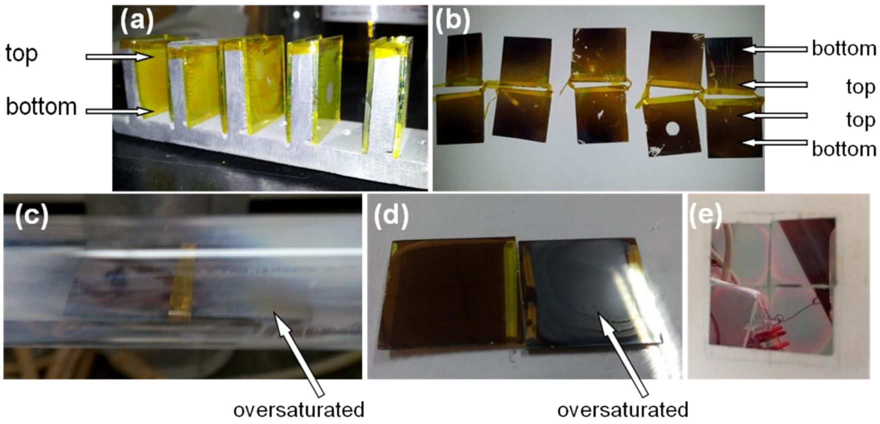

Fig. S1 Photographs of substrates of different orientations in two types of tubular LPCVD apparatus: (a) PbI_2 films vertically stacked on an aluminum holder and, (b) the corresponding perovskite films; (c and d) perovskite films horizontally stacked on an aluminum holder; and (e) uniform perovskite films fabricated using the PHP apparatus.

Besides the PHP apparatus discussed in the main text, we also constructed two types of tubular apparatus to synthesize perovskite thin films. Each apparatus consists of a glass tube, in which the substrates are stacked either vertically (Fig. S1a and b) or horizontally (Fig. S1c and d). Temperatures of the wall of the tube and the substrate holder were controlled separately. Operations are the same for both reactor geometries.

MAI powders were uniformly placed on the bottom of the tube. After setting PbI_2 substrates onto the substrate holder, the apparatus was pumped down to a pressure of about 100 Pa. Efficient evaporation of MAI requires about 130 ^{o}C (see thermal gravimetric analysis in Fig. S3). Therefor, the temperatures of the wall and the substrate holder were ramped up to nominal temperatures of 130 °C and 120 °C, respectively. The temperature of the wall of the tube could be precisely maintained at 130 ^{o}C during the reaction. However, the temperatures of the substrate holders rose along the reaction time, caused by the heat transfer from hot MAI molecules, and reached about 150 ^{o}C in half an hour. Increasing the reaction time led to even higher final temperature of the holder.

As the reaction proceeded, the samples exhibited colour gradients along the substrate edge and the tube length (Fig. S1 b). The top area shown in Fig. S1 b that is far from the MAI source is relatively undersaturated of MAI compared to the bottom area. In the horizontal direction, the farther film is mirror-like, whereas the nearer one has become oversaturated. In both cases it is obvious that the colour of films closer to the MAI source darkened first and also bleached first (Fig. S1 c). The hazy film on the right marked with arrows was closer to the MAI source, compared to the mirror-like film on the left (Fig. S1 d). This means that the extent of reaction depends on the distance from the MAI source. These issues lower controllability and reproducibility of the films and devices.

Fortunately, these issues could be overcomed using the PHP apparatus. Perovskite films synthesized using the PHP method are uniform (Fig. S1 e), because of the uniform loading of MAI on different films. On average, solar cells based on the perovskite films fabricated using the tubular LPCVD performed worse than these via PHP. The best device fabricated using the tubular LPCVD had a PCE of 8.1%, with a J_{SC} of 19.0 mA cm^{-2}, V_{OC} of 0.80 V, and FF of 0.53 (Fig. S2). Note the optimal reaction time of the tubular LPCVD method is 30 min, much shorter than the 120 min of the PHP method. The fast reaction rate is probably a consequence of the gradually increased temperature of the substrate holder. However, the accelerated reaction is actually detrimental to the coalesce of grains in the perovskite films.[1]

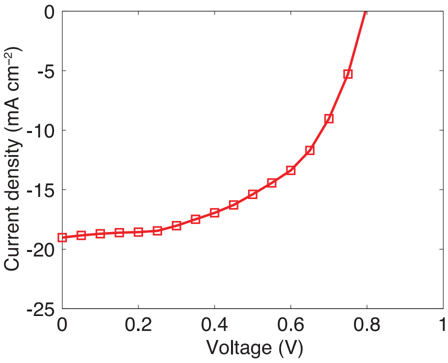

Fig. S2 *J*-*V* curve of a representative device with the perovskite layers synthesized via the tubular LPCVD method in 30 min. The structure of the device is the same as the devices fabricated via PHP.

On the contrary, perovskite grains have enough time to coalesce in PHP. The bottom plate can stay at constant temperature during the entire reaction process because it is thermally isolated from the top plate and large enough to resist the heat received from the MAI molecules. The PHP apparatus is advantageous not only due to its precise control of temperatures but also due to its uniform and controllable loading of evaporated MAI onto PbI_2 substrates.

Simulation of thickness distribution

Consider two possible vacuum levels that the vacuum chamber could reach during operation, including high vacuum (for example 10^{-4} Pa) if a turbo molecular pump was used and low vacuum (for example 1~100 Pa) if only a mechanical oil pump was used. In the first case, three assumptions were made to estimate the uniformity of a MAI film deposited on the bottom hot plate. First, the distribution of evaporation rate is uniform over the entire top plate, which can be realized by rotating the plate during spray coating. Second, the thermally evaporated MAI particles transport without collision between the plates, meaning that the mean free path λ of MAI molecules is far larger than the source-substrate distanced. Third, the top plate is an ideal surface evaporation source, i.e. following cosine distribution, in which the film thickness decreases with the distance from the center of substrate x according to

$$\frac{t}{t_0}=\frac{1}{\left[1+\left(\frac{x}{h}\right)^2\right]^2}$$

In the second cases, the mean free path λ of MAI molecules is the same order of magnitude as the source-substrate distance d. For simulation, we further presume that molecules will diffuse back and condense on the top plate if they are scattered during the transport between the top and the bottom plates. According to the scattering theory, the possibility of a molecule evaporated from the top plate can reach the bottom plate is

$$P=e^{-\frac{l}{\lambda}}$$

where l is the distance between the evaporation point and the condensation point. The red dashed curve in Fig. S4a is the simulation using the above four assumptions and with λ equals 0.5 mm. It shows an even higher degree of uniformity than in PVD (the black curve).

Extraction of the UV-visible absorption edges

We extract the absorption edges of perovskite films around 480 nm according to the methods shown in Fig. S3. First, the gradient (green curve) of the absorption spectrum (red curve) is calculated. Then the maximum and the minimum points (vertical arrows) of the gradient in the range from 450 to 525 nm are used to plot the tangent lines of the absorption spectrum (dashed lines). The intersection point of the two tangent lines represents the edge of the absorption plateau.

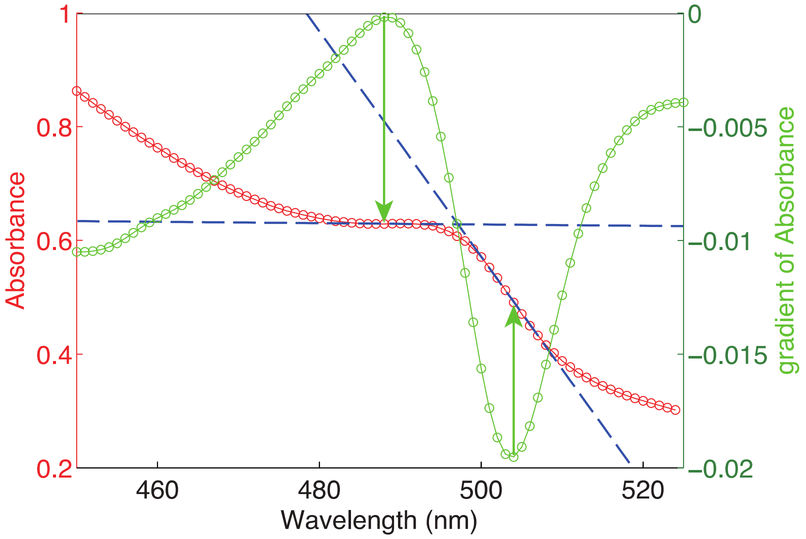

Fig. S3 A method for extracting the absorption plateau edge of perovskite films around 480 nm.

Estimation of crystalline diameters using Scherrer equation

The crystalline diameter D was estimated using the Scherrer equation**:** $D = K^*\lambda/(\beta^*\cos\theta)$, where K is a dimensionless shape factor with a value close to unity but varies with the actual shape of the crystallite; λ is the X-ray wavelength; β is the line broadening at half the maximum intensity (FWHM), after subtracting the instrumental broadening, in radians; θ is the Bragg angle, K is set to 0.843 (assume spherical crystals with cubic symmetry),[2] λ is set to 0.15405 nm and θ is set to 7.04°, corresponding to the (110) reflection at 2θ = 14.08°.

Supporting Table 1 Estimated particle sizes in thin films of $MAPbI_3$ under variable vapor growth time conditions. The average particle sizes were estimated using the Scherer equation using a constant shape factor of K = 0.834 for the (110) reflection at 2θ = 14.08°. Instrumental broadening of 0.08° was calculated using polycrystalline silicon as standard.

Time (min)	30		60		120		150	
Substrate	ITO	PEDOT:PSS	ITO	PEDOT:PSS	ITO	PEDOT:PSS	ITO	PEDOT:PSS
β	0.2071	0.1986	0.1322	0.1333	0.5499	0.1320	0.1605	0.1550
D (nm)	79.7	85.4	194.0	189.9	21.5	194.9	125.8	135.0

Extensive Figures and Table

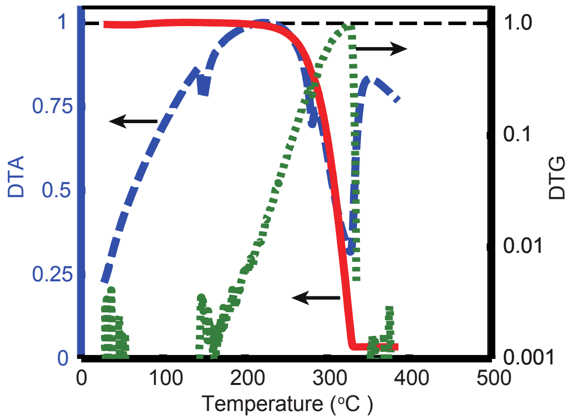

Fig. S4 Thermal properties of MAI in N_2: differential thermal analysis (DTA, blue), thermal-gravimetric analysis (TG, red), and differential thermal-gravimetric analysis (DTG, green). Thermal properties of MAI (5 mg) were measured in N_2 using a thermogravimetric analyzer (TG/TA6300, Seiko) in the heating range of 30-400 °C and the heating ramp was 10 °C/min. The lowest temperature required for appreciable evaporation of MAI was found to be 130 °C.

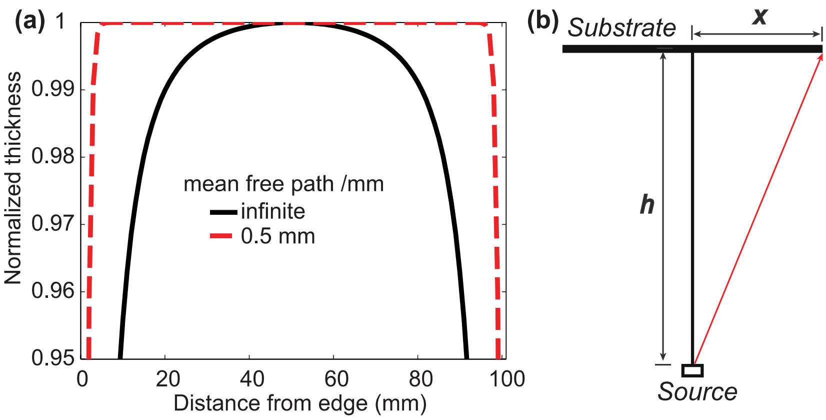

Fig. S5 (a) Distribution of normalized film thicknesses on the bottom plate with different mean free paths; (b) Schematic illustration for the determination of thickness distribution.

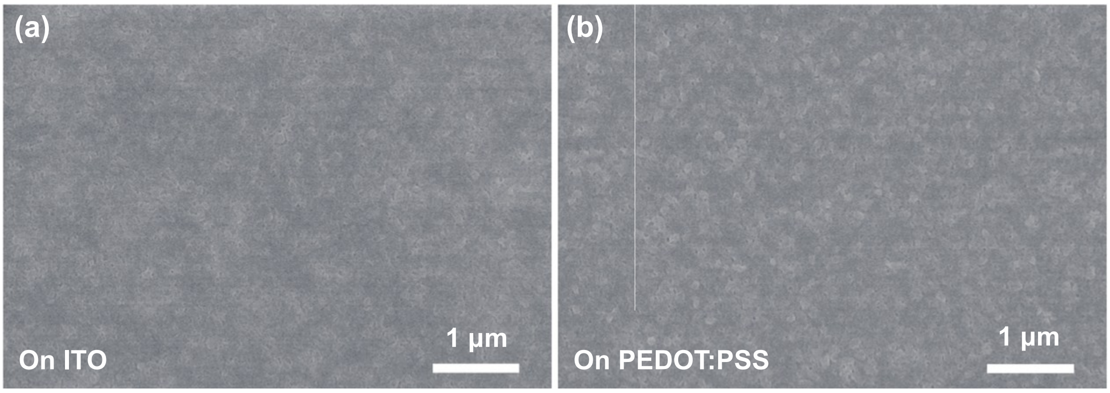

Fig. S6 (a) SEM images (×50000) of PbI_2 films on ITO substrates; (b) on PEDOT:PSS substrates.

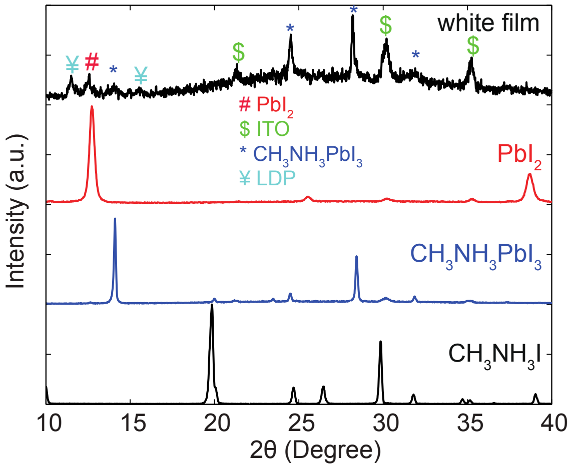

Fig. S7 XRD patterns of PbI_2, $MAPbI_3$, MAI films, and a white-color perovskite thin film on ITO.

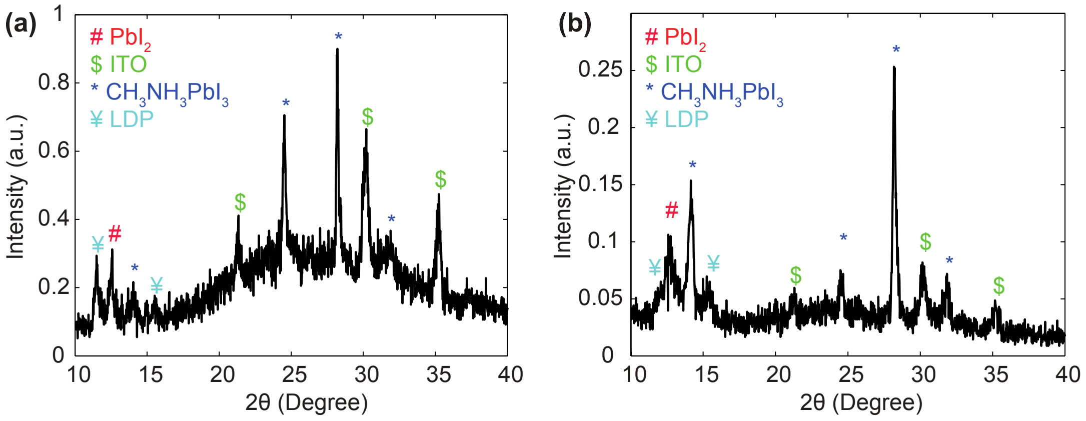

Fig. S8 (a) Zoomed XRD pattern of the white-color perovskite film on ITO after absorbing excess MAI shown in Figure 2a; (b) Zoomed XRD pattern of the perovskite film on ITO reacted in 120 min shown in Figure 5a.

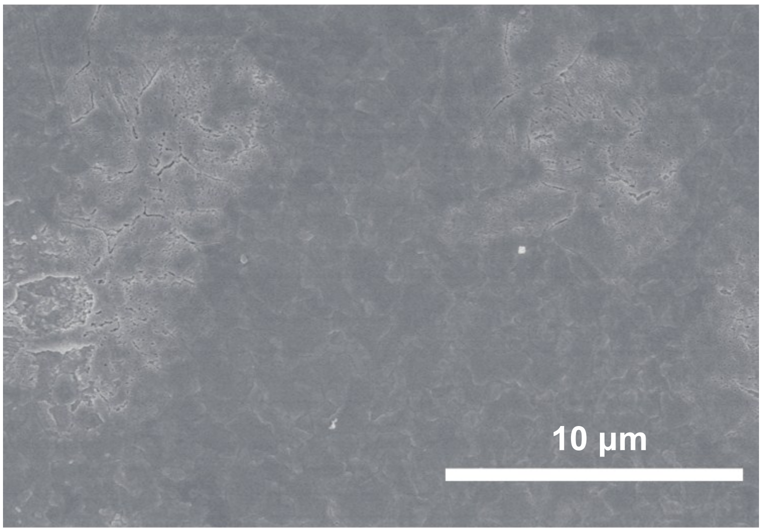

Fig. S9 SEM image (×5000) of a white perovskite film on ITO reacted in 120 min after being rinsed with isopropanol.

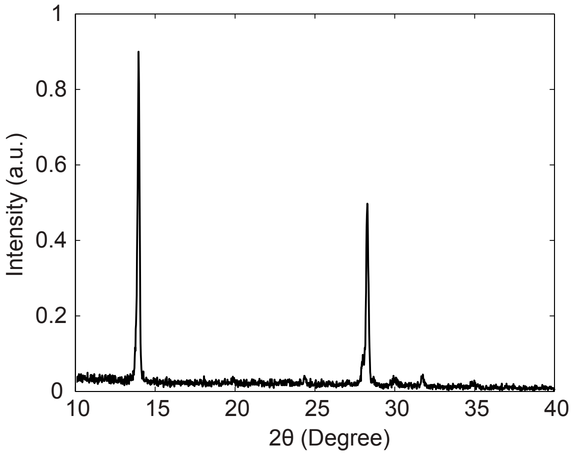

Fig. S10 XRD pattern of a device without the aluminium electrode, i.e., BCP/C60/PCBM/perovskite/PEDOT:PSS/ITO. It shows that MAPbI3 were well crystallized.

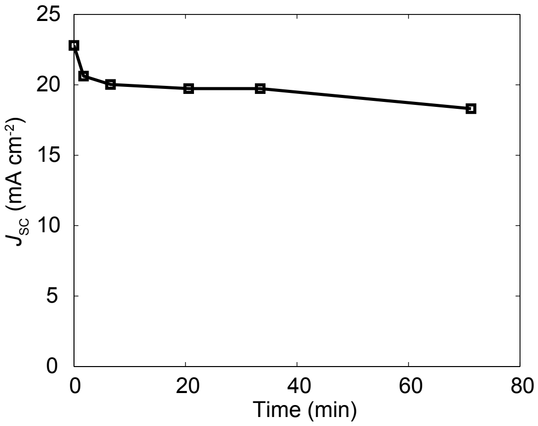

Fig. S11 Repetitively tested short circuit current density of a solar cell stored under simulated AM1.5 solar light.

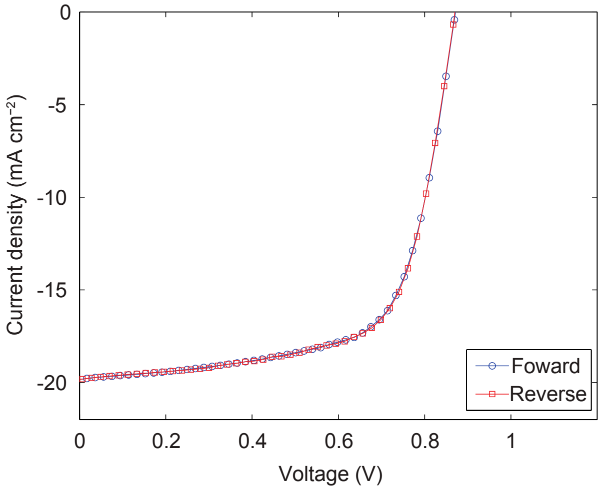

Fig. S12 *J-V* curves of a perovskite solar cell measured with the bias scanned in different directions.

Supporting Table 2 Key parameters of a PSC measured with the bias scanned in different directions.

	J_{SC} (mA cm^{-2})	V_{OC} (V)	FF	PCE (%)
Reverse	19.8	0.870	0.672	11.6
Forward	19.8	0.871	0.668	11.5

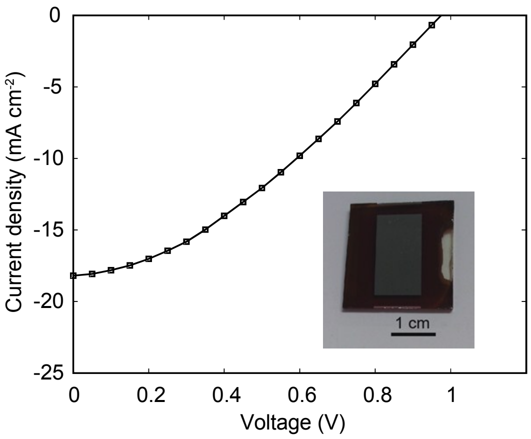

Fig. S13 *J-V* curves of a perovskite solar cell with an active area of 1.5 cm^2. V_{OC} was 0.98 V, J_{SC} 18.2 mA cm^{-2}, and FF 0.34.

References

1. P. Luo, Z. Liu, W. Xia, C. Yuan, J. Cheng, and Y. Lu, *ACS Appl. Mater. Interfaces*, 2015, **7**, 2708–14.

2. J. I. Langford and A. J. C. Wilson, *J. Appl. Crystallogr.*, 1978, **11**, 102–113.